H^{∞} CONTROL OF MILLING AMB SPINDLE

Kenzo Nonami * , ***Hirochika Ueyama*** ** ***and Yutaka Segawa*** *

* *Chiba University,1-33 Yayoi-cho, Inage-ku, Chiba 263, Japan*
** *Koyo Seiko Co., Ltd.24-1 Kokubutojyo-cho,Kashiwara-shi, Osaka 582, Japan*

ABSTRACT

This paper is concerned with the DSP-based H^{∞} control of the actual milling AMB spindle rotor systems. The H^{∞} control systems are designed for all five-axis-control of one axial direction and four radial directions. Then we tried some simulations comparing with conventional PID control. Next, we tried the experiments using DSPs of TMS320C30 and TMS320C40 in cases of levitations and rotations. In experiments with parameter variations of increment of rotor mass, which is called robust performances, it has been clarified that the H^{∞} control system is superior to conventional PID control system. We successfully ran up to about 35000 rpm with very small vibration and also safety. The control performances in high speed rotations, in particular, the envelop of amplitudes at sensor locations depending on rotational speed are almost the same as PID control.

1. INTRODUCTION

The research works concerned with magnetic bearing have been agressively carried out these days. In particular, some of the recent research subjects and topics may be listed as follows; (1) Studies on shifts from the conventional analog control to digital control. (2) Studies on shifts from the stabilization control of PID control to advanced control in which modern control theory, robust control theory, and learning control are applied. (3) Studies of flexible rotor - magnetic bearing systems which pass higher-order flexible modes. (4) Studies of sensorless magnetic bearings, (5) Studies for the joint use as magnetic bearings for levitation and also motor stator for rotation, (6) zero-power magnetic bearings, superconducting bearings, etc.

In the field of control theory, robust control is one of the biggest topics in recent years and many application studies of robust control theory are carring out [1,2,3]. H^{∞} control theory proposed by Zames is well known as the typical robust control theory for linear control and is very powerful control system design method for actual plants because of existence of excellent CADs as computer aided control system design(CACSD). H^{∞} control theory includes a frequency shaping in classical control theory and an optimization in modern control theory like LQG. Therefore, H^{∞} control theory is situated in the center of robust control theory and post modern control theory.

This paper is concerned with (1) and (2) above mentioned. In particular, we have designed H^{∞} control system for actual milling AMB spindle. These H^{∞} control system based on the two block mixed sensitivity problem regarding as the standard H^{∞} control problem is designed for this AMB system by taking into account unknown higher order flexible modes and unknown disturbances of the plant. The state space model for the full order system of the flexible rotor is derived using finite element method. Also the reduced order model for controller design is given by eliminating every flexible mode of this rotor because the operating speed of this rotor is under the first bending mode. After designing the continuous time H^{∞} controller with fourteenth-order which is similar to conventional analog PID controller through adjusting frequency-dependent weighting functions, we digitized the continuous time H^{∞} controller to discrete time H^{∞} controller using a bilinear transformation method. We have succeeded the rotation test up to 35000 rpm. We have concluded that the DSP based H^{∞} control system designed by us for the milling AMB spindle has good performances and robustness comparing with a conventinal PID control system.

2. MODELLING OF FLEXIBLE ROTOR MAGNETIC BEARING SYSTEMS

2.1 Modelling in Axial Direction

Figure 1 shows the dynamical model with one-axis control type in the axial direction of the magnetic bearing. The state equation and the output equation are given by Fig.1 as follows;

$$\dot{X} = Ax + Bu \qquad (1)$$
$$y = Cx$$

where,

$$A = \begin{bmatrix} 0 & 1 \\ a_1/M & 0 \end{bmatrix},\ B = \begin{bmatrix} 0 \\ a_2/M \end{bmatrix},\ C = [1\ 0],\ x = \begin{bmatrix} x_1 \\ x_2 \end{bmatrix}$$

$$a_1 = 2\frac{2p_0}{x_0},\ a_2 = 2\frac{2p_0}{i_0},\ p_0 = k_a\frac{i_0^2}{x_0^2}$$

The notations are M ; the mass matrix, x_1 ; the displacement of the mass, x_2 ; the velocity of the mass, k_a ; the attractive force coefficient, p_0 ; the bias attractive force, i_0 ; the steady-state current, x_0 ; the steady state gap. Table 1 shows the parameter values in the axial direction of the magnetic bearing.

We made the model concerning an eddy current loss of the magnetic bearing in the axial direction as follows;

$$G_M = \frac{6.8\times10^5 s^2 + 6.3\times10^8 s + 4.5}{4.3\times10^3 s^3 + 3.5\times10^7 s^2 + 5.2\times10^9 s + 1.9\times10^{11}} \qquad (2)$$

Finally, we used the extended state equation and output equation including Eq.(1) and Eq.(2) as follows;

$$\dot{x}_a = A_a x_a + B_a u \qquad (3)$$
$$y_a = C_a x_a$$

2.2 Modelling in Radial Direction

Figure 2 shows the flexible rotor model. Table 2 shows the parameter values of the magnetic bearing system in the radial direction. In this case, the discrete mass model shown in Fig.2 is applied using a finite element method. The state equation taking into account the electromagnetic forces and the truncation of every flexible mode is described for only the rigid mode.

Table 1 Parameters in axial direction of milling AMB spindle

Parameter		Value	Unit
Mass	M	7.84458	kg
Gap	$h0$	0.3	mm
Bias current	$i0$	0.8	A
Bias attractive force	$p0$	56.889	N
Magnetic constant	k_a	8.0	N · mm²/A²
Sensor	Gs	10000	V/m

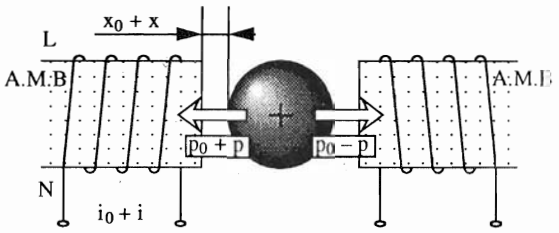

Fig.1 Model of magnetic bearing in axial direction of milling AMB spindle

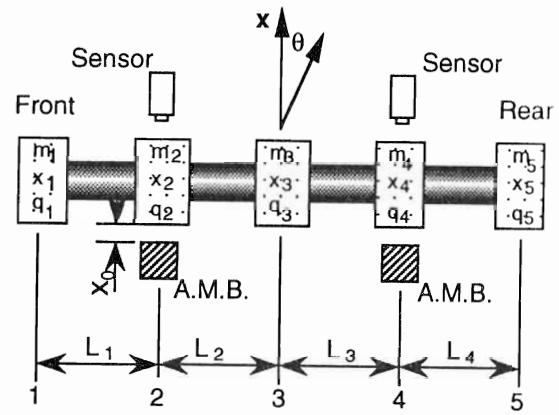

Fig.2 Equivalent flexible rotor model of milling AMB spindle

Table 2 Parameters in radial direction of milling AMB spindle

Parameter		Value	Unit
Mass	$m1$	1.22	kg
	$m2$	2.29	kg
	$m3$	1.55	kg
	$m4$	1.8	kg
	$m5$	0.98457	kg
Length	$L1$	76.0	mm
	$L2$	90.0	mm
	$L3$	132.0	mm
	$L4$	28.0	mm
Diameter	d	59.4	mm
Damping constant	ζ_i $(i = 1, \cdots, 10)$	0.002	
Gap	$h0$	0.3	mm
Bias current	$i0f$	0.3	A
	$i0r$	0.5	A
Bias attractive force	$p0f$	23.54	N
	$p0r$	21.939	N
Magnetic constant	k_af	23.54	N · mm²/A²
	k_ar	7.898	N · mm²/A²
Sensor	Gs	10000	V/m

$$\dot{x}_r = A_r x_r + B_r u$$
$$y_r = C_r x_r \qquad (4)$$

Where, Eq.(4) includs the characteristics of low-pass filter in addition to the rigid rotor-magnetic bearing systems because we also take into account the characteristics of actuator and power amplifier like the axial direction.

3. DESIGN OF PID CONTROL AND H^∞ CONTROL AND THEIR PERFORMANCES BY SIMULATIONS

3.1 PID Control in Axial Direction

A magnetic bearing sysytem should be stabilized at first. The designed PID controller is finally as follows;

$$K_a = k_p + k_i + k_d$$
$$= 2.35 + 3.33 \times \frac{10.6}{s} + \frac{213000s}{(s+10000)(s+2130)} \qquad (5)$$

Next, we digitized the PID controller of Eq.(5) using bilinear transformation with the sampling time 0.1msec. Figure 3(a) shows the bode diagram of the discrete time PID controller. Figure 4(a) shows the impulse response in levitation using the controller of Fig.3(a).

3.2 H^∞ Control in Axial Direction

We apply a mixed sensitivity problem to design the H^∞ control system for this plant. The mixed sensitivity problem is well known as a fundamental design method for H^∞ control. We also applied the stability degree specification method and so on for this. The results coincided with the mixed sensitivity problem.

In the case of the mixed sensitivity problem, the cost function is as follows;

$$J = \left\| \begin{matrix} W_1(s)N(s) \\ W_2(s)M(s) \end{matrix} \right\|_\infty < 1 \qquad (6)$$

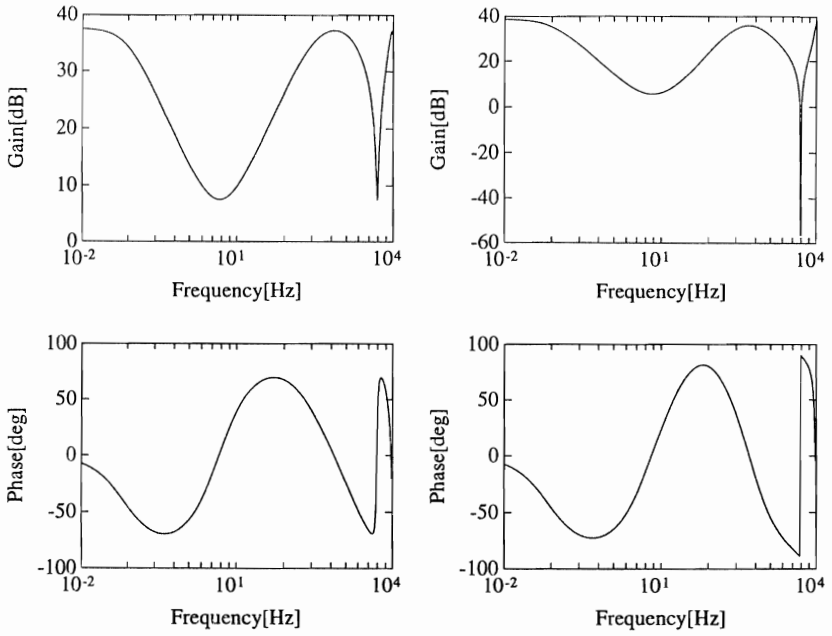

(a) discrete time PID controller *(b) discrete time H^∞ controller*

Fig.3 Discrete time PID controller and H^∞ controller with sampling time 0.1 msec in axial direction

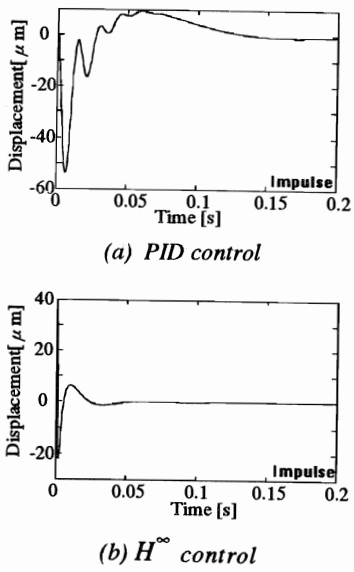

(a) PID control

(b) H^∞ control

Fig.4 Impulse time history responses

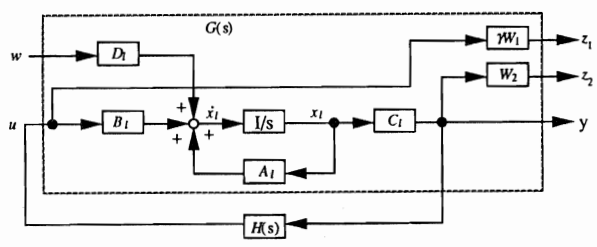

Fig.5 Generalized plant and H^∞ controller

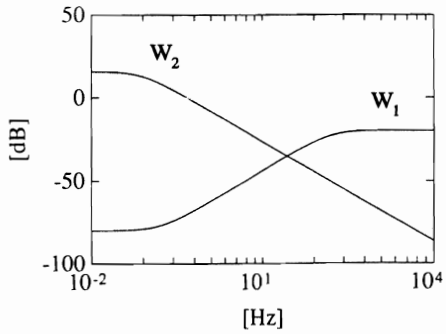

Fig.6 Frequency weighting functions for axial direction

where, $W_1(s)$ is the frequency weighting function used for robust stabilization in higher frequencies and $W_2(s)$ is for sensitivity reduction and should be determined to have an integrator for the H^∞ controller in lower frequency region. And $N(s)$ and $M(s)$ are obtained using Fig.5 of a generalized plant with H^∞ controller.

$$N(s)=H(s)[I-P_a(s)H(s)]^{-1}P_a(s)$$
$$M(s)=[I-P_a(s)H(s)]^{-1}P_a(s) \quad (7)$$

where $P_a(s)$ is defined as follows;

$$P_a(s)=C_a(sI-A_a)^{-1}B_a \quad (8)$$

The frequency weighting functions $W_1(s), W_2(s)$ are selected with try and error as follows;

$$W_1(s)=\frac{0.1(s+1)}{s+1000},\quad W_2(s)=\frac{3}{s+0.5} \quad (9)$$

Equation (9) is shown in Fig.6. The continuous time H^∞ controller is easily designed using Fig.5 and MATLAB. Figure 3(b) shows the digitized bode diagram of the H^∞ controller with a sampling time 0.1 msec. The compensator is the seventh-order system. It is found that the H^∞ controller is very similar to the PID controller comparing Fig.3(b) with Fig.3(a). The impulse response in levitation is shown in Fig.4(b). Figure 4(b) is superior to Fig.4(a) concerning a settling time and a maximum amplitude.

3.3 PID Control in Radial Direction

Figure 7(a) shows the bode plots of the eighth-order digitized PID controller with a sampling time 0.3 msec.

3.4 H^∞ Controller in Radial Direction

We selected the frequency weighting functions like

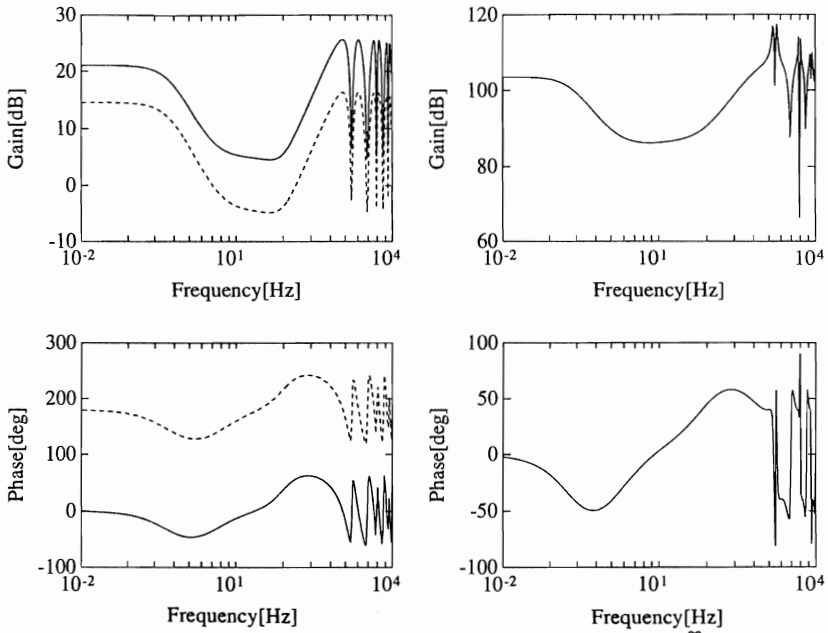

(a) discrete time PID controller *(b) discrete time H^∞ controller*

Fig.7 Discrete time PID controller and H^∞ controller with sampling time 0.3 msec in radial direction

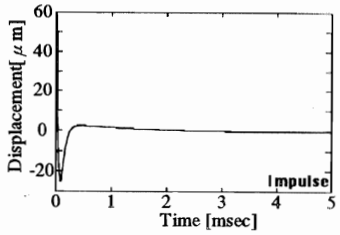

Fig.9 Inpulse time history responses

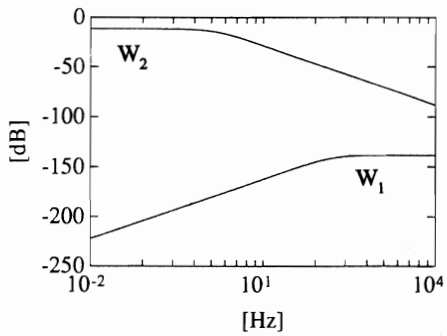

Fig.8 Frequency weighting functions for radial direction

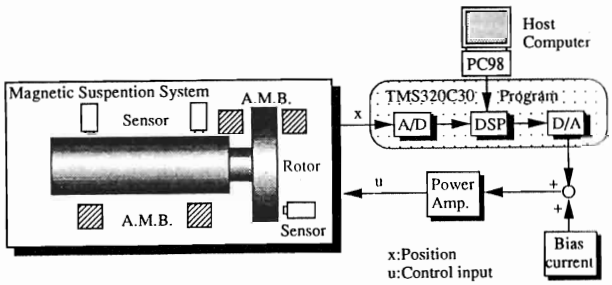

Fig.10 Configuration of DSP-based H^∞ control system

Fig.8. The fourteenth-order discrete time H^∞ controller with a sampling time 0.3 msec is shown in Fig.7(b). The H^∞ controller is given by bilinear transformation of the continuous H^∞ controller. Figure 9 shows the time history response added an impulse disturbance in levitation.

4. EXPERIMENTS

We used the actual milling AMB spindle for experiments of H^∞ control and installed the H^∞ controller designed in Chapter 3 to DSP and carried out the experiments comparing with analog PID control. Figure 10 shows the schematic block diagram of digital control system in the case of radial direction using DSP-based H^∞ control. Two displacements measured by two sensors in the radial direction go to DSP (TMS320C30) through A/D converter and two control inputs made by DSP are supplied to two electromagnets as actuators through D/A converter and power amplifiers. Two independent H^∞ controllers are used for the x direction and the y direction each other because we assume the uncoupled system for two directions.

4.1 Experiments in Axial Directions

The impulse response in levitation using the analog PID controller is shown in Fig.11. Figure 12 shows the impulse response using the H^∞ controller. It seems that these are almost the same data. However, the stiffness in the case of the PID control is stronger than H^∞ control.

4.2 Experiments in Radial Directions

Each direction is controlled by each DSP (TMS320C30) independently. The sampling time was 0.3 msec (sampling frequency 3.3 KHz) in that case. We have already succeeded the experiments using only one DSP based on TMS320C40 with sampling time 0.125 msec (sampling frequency 8 KHz). Namely, the five-axis including four-radial-axis and one-axial- axis is controlled by only one DSP(TMS320C40).

Figure 13 shows the impulse response in the case of the analog PID control and Fig.14 is in the case of H^∞ control. These are very different responses. The performance of H^∞ control is very well and damped quickly. Next, we verified a robustness varying mass of the rotor at lift off. The nominal rotor mass is 7.8 Kg.

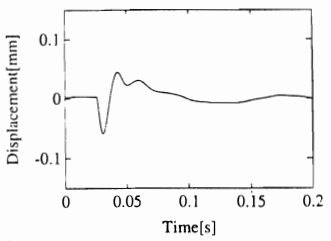

Fig.11 Impulse time history responses using analog PID control in axial direction

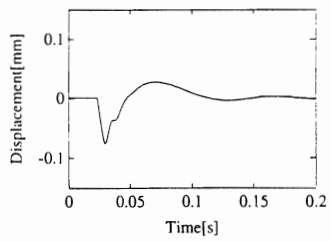

Fig.12 Impulse time history responses using digital H^∞ control in axial direction

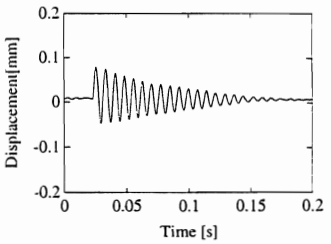

Fig.13 Impulse time history responses using analog PID control in radial direction

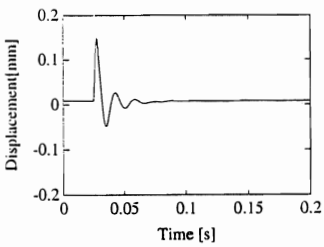

Fig.14 Impulse time history responses using digital H^∞ control in radial direction

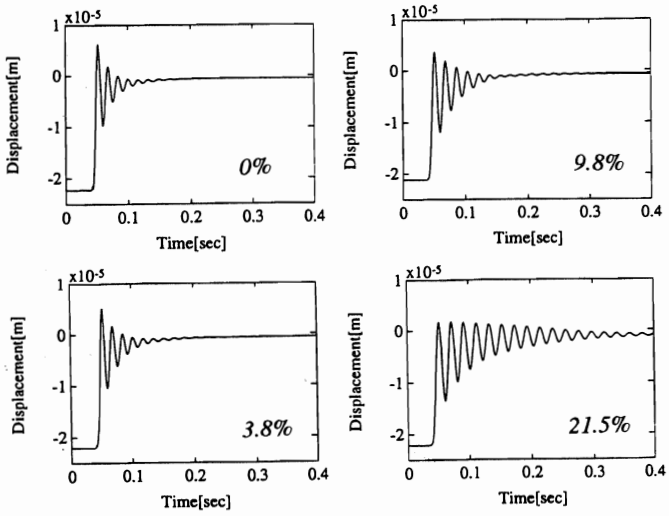

Fig.15 Step responses using analog PID control for parameter variations from 0% to 21.5%.

We varied the added mass of rotor from 0%, 3.8%, 9.8% 21.5%. Figures 15 shows the step responses in the cases of PID control for parameter variations above mentioned. It is so clear that control performances, namely robust performances, are influenced by pertubations of mass increment. On the other hand, Fig. 16 shows the cases of H^{∞} control. H^{∞} control system is also changed. However, it seems that the PID control system has higher sensitivity for variation of the rotor mass comparing with H^{∞} control.

We have already done the high speed rotation test up to 35000 rpm in the case that rotor is supported by the H^{∞} controller. Figure 17 shows the orbits for 15000rpm, 20000rpm, 25000rpm, 30000rpm using the PID controller and Fig.18 is the case of the H^{∞} control. These maximum amplitudes are approximately 2μ m. We can conclude that theses are almost the same performances.

5. CONCLUSIONS

We have succeeded the rotation test up to 35000 rpm using H^{∞} controller designed with a standard mixed sensitivity problem. And, we have concluded that the DSP-based H^{∞} control system designed by us for the milling AMB spindle has good performances and robustness comparing with a conventinal PID control system. In particular, it seems that the H^{∞} control is superior to the PID control because the PID is analog control in this case and the H^{∞} control is digital. However, we cannot recognize the definite different performances between PID control and H^{∞} control yet. We continue this research work to design an advanced H^{∞} control system now.

REFERENCES

[1]Cui W. and Nonami K., H^{∞} Control of Flexible Rotor-Magnetic Bearing Systems, Proc.of the 3rd Int Sym. on Magnetic Bearings,505-512, 1992

[2]Nonami K., Wang J., Sampei M and Mita T., Active Vibration Control of a Flexible Rotor Using H^{∞} Control Theory , Proc. of the ASME Design Conf. on Rotating Machinery and Vehicle Dynamics,DE-35,85-92, 1991

[3]Nonami K. and Ito T., μ Synthesis of Flexible Rotor Magnetic Bearing Systems, Proc. of the 4th Int. Sym. on Magnetic Bearings,1994

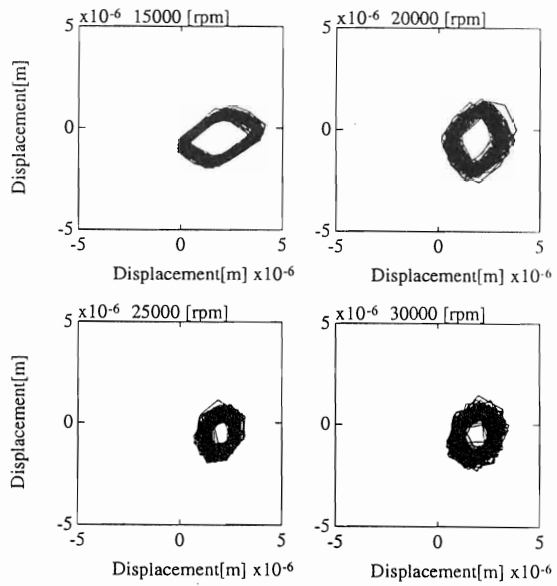

Fig.17 Orbits for high speed rotation test using analog PID

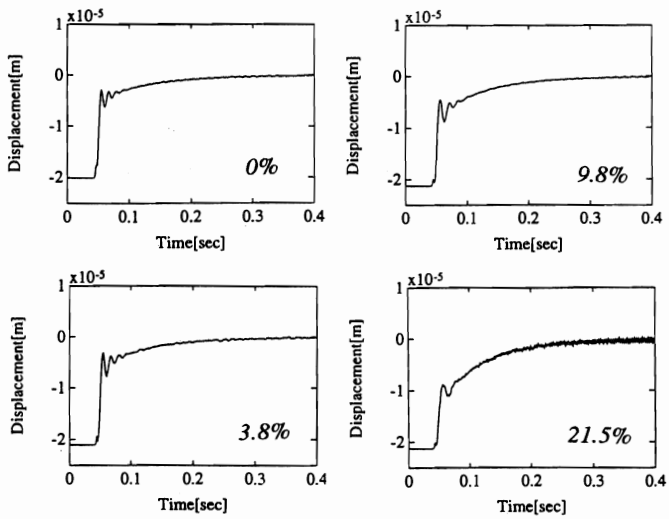

Fig.16 Step responses using digital H^{∞} control for parameter variations from 0% to 21.5%.

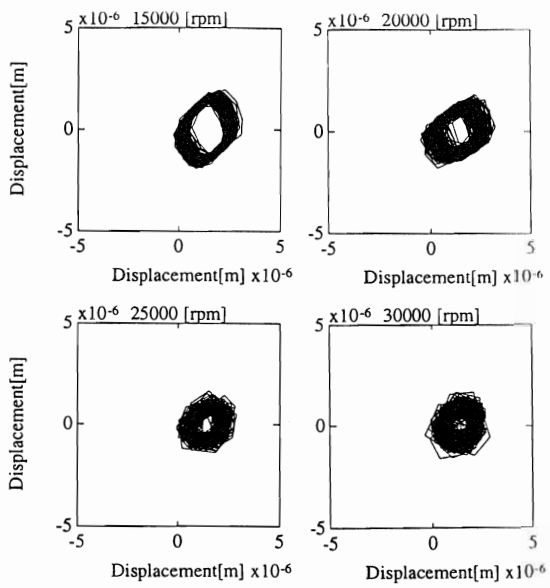

Fig.18 Orbits for high speed rotation test using digital H^{∞} control

AXIAL AND RADIAL FORCES ON A PUMP IMPELLER OBTAINED WITH A MAGNETIC-BEARING FORCE MEASUREMENT RIG

Adiel Guinzburg
Frederic W. Buse
Advanced Technology, Corporate Technology
Ingersoll-Dresser Pump Company, Phillipsburg, NJ, USA

ABSTRACT
An experiment was designed to measure the forces and moments that result from the hydrodynamic interactions in a centrifugal pump. In the past, experimental evaluation of the hydraulic forces and moments on impellers has been accomplished via techniques such as strain measurements and static pressures at taps in the walls adjacent to the impeller. The present experimental results are obtained using the magnetic bearing test rig in the Corporate Applied Research Laboratory of the Ingersoll-Dresser Pump Company. In the paper we present the comparison between the results for the single stage pump obtained by the traditional methods and those derived from magnetic bearing reactions. The results are given for the full range of flowrates from shutoff to runout.

INTRODUCTION
Hydrodynamic interactions in centrifugal pumps have typically focused on the radial and axial forces. Because of the uneven distribution of the pressure on the shroud in single stage end suction pumps, there is an additional component which manifests itself as a moment (Buse [1979]). This may lead to increased shaft deflection, shaft stress and decreased bearing life.

This study investigates the forces and moments that result from the hydrodynamic interactions in a centrifugal pump. The impeller and the spiral casing are designed to provide circumferentially uniform discharge flow pattern at design conditions. However at off-design conditions, the discharge flow pattern is no longer uniform; when the flowrate changes the discharge conditions become asymmetric. This results in a net radial force due to the asymmetric pressure discharge condition. Note that even at the design flowrate, the discharge conditions could be asymmetric if the impeller is displaced from the design center by shaft deflection or bearing wear.

There are two sources that contribute to the radial hydrodynamic forces on an impeller. One is due to the asymmetric distributions around the impeller and the other is caused by the asymmetric momentum fluxes at the impeller inlet and discharge. The first contribution can be evaluated by integrating the asymmetric pressure distribution around the inlet and discharge of the impeller. There is a negligible contribution from the net of the momentum fluxes.

BACKGROUND
The forces are defined by expressing the instantaneous forces, $F_x(t)$, $F_y(t)$ and $F_z(t)$ (figure 1) acting on the impeller in the linear form:

$$\begin{pmatrix} F_x \\ F_y \\ F_z \\ m_x \\ m_y \end{pmatrix} = \begin{pmatrix} F_{ox} \\ F_{oy} \\ F_{oz} \\ m_{ox} \\ m_{oy} \end{pmatrix} + [A] \begin{pmatrix} x(t) \\ y(t) \\ z(t) \\ \theta_x(t) \\ \theta_y(t) \end{pmatrix} \qquad (1)$$

The first term on the right hand side represents the steady, time-averaged forces in a stationary frame and [A] is the rotordynamic matrix where x(t), y(t), z(t) are the shaft displacements from the mean position. The steady radial forces F_{ox}, F_{oy}, F_{oz} result from asymmetries in the flow and have been measured by several authors: (Iversen et al. [1960], Agostinelli et al. [1960], Domm and Hergt [1970], Chamieh et al. [1985], Adkins [1985]. The rotordynamic matrix [A]

will in general be a function not only of the mean flow conditions and pump geometry but also of the whirl motion. Rotordynamic forces imposed on a centrifugal pump by the fluid flow through it were first measured by Domm and Hergt (1970), Hergt and Krieger (1969-70), Chamieh et al. (1985) and Jery et al. (1985).

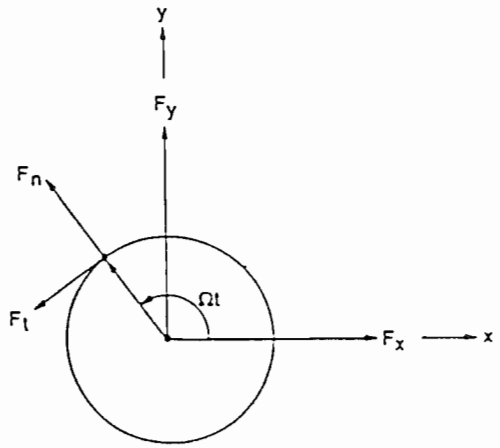

FIGURE 1: Schematic of the Fluid Forces on a Pump.

For the present discussion, the emphasis will be on the steady forces. There are several empirical relationships which are used by pump designers to estimate these forces. These approximations gloss over the differences between an open impeller versus a closed impeller, or the influence of scallops in the impeller disk (figure 2) on the load. In the present paper, the loads derived from the magnetic bearing will be presented and compared with the empirical results.

Radial Force

The magnitude and location of the radial force acting on the impeller depends on the operating point relative to the best efficiency point (BEP) and specific speed. It is usually a minimum at best efficiency and a maximum at shutoff.

$$F = P.D_2.b_2.K \qquad (2)$$

where

b_2 is the overall impeller width, including shrouds.

D_2 is the impeller diameter.

F is the radial force.

P is the developed pressure.

K is an empirical constant.

The earliest correlation for the radial load on a centrifugal pump was by Stepanoff (1957) who estimated the empirical constant as a function of the capacity:

$$K = 0.36\left(1 - \left(\frac{Q}{Q_n}\right)^2\right) \qquad (3)$$

where

Q is the flowrate where the force is evaluated.

Q_n is the flowrate at the best efficiency point.

Subsequently, K-values for a single spiral volute were determined experimentally by Agostinelli et al. (1960) as a function of flow *and specific speed.* This observation was important as the specific speed characterizes the impeller geometry. Biheller (1965) also presented a semi-empirical relation for the radial load in a slightly different form.

Axial Force

The classic equation for the axial force is a function of the developed pressure and does not account for changes with flowrate or specific speed. The following equation describes the axial force as the difference between the axial force generated on the front shroud and the axial force on the back shroud:

$$F_z = P.\left[\left(\frac{K_2+K_1}{2}\right)(A_2 - A_1) - \left(\frac{K_2+K_h}{2}\right)(A_2 - A_h)\right] \qquad (4)$$

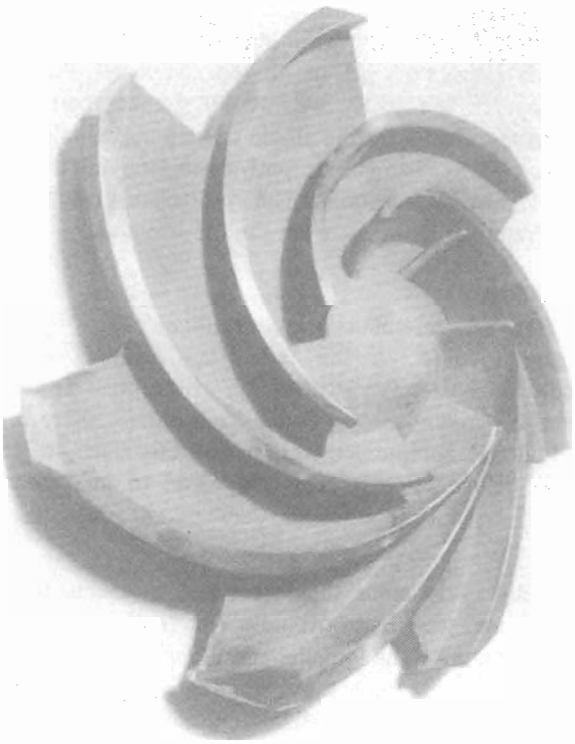

FIGURE 2: Test Impeller. Note scallops in Impeller Disk.

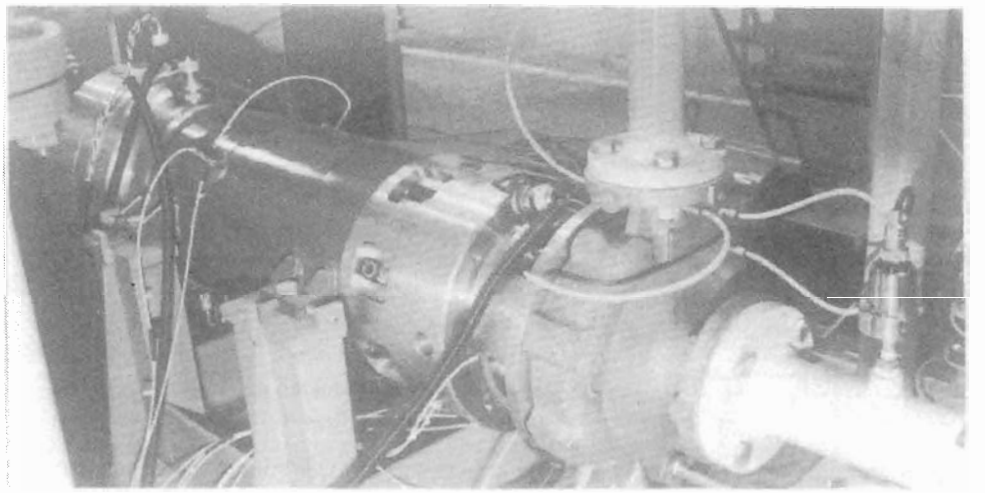

FIGURE 3: Magnetic Bearing Test Rig at Ingersoll-Dresser Pumps with a Centrifugal Pump in the Foreground.

where

k_1 and k_2 represent the ratios of the head at the impeller diameter relative to the total head.
k_h represents the ratio of the head at the hub diameter relative to the total head.

Impeller designs employ back vanes, back rings, balance holes or scalloping as a means to reduce the axial thrust. The following table demonstrates the effect of these configurations on the force.

Table 1: Empirical determination of axial force.

Configuration	K_h
Plain shroud	0.4
Back vanes	0.1 to 0.25
Back ribs with balance holes	0.1
Back ring	0.6 to 0.7

EXPERIMENTAL FACILITY

In the past, experimental evaluation of the hydraulic forces and moments on impellers has been accomplished via techniques such as strain measurements and static pressures at taps in the walls adjacent to the impeller. Previous testrigs (Chamieh et al. [1985], Bolleter et al. [1985], and Ohashi and Shoji [1987]) required slipring assemblies to transport the force signal from the rotating member to the acquisition system. The advantage of an active magnetic bearing concept is that the fluid-structure interaction problems in pumps, compressors, turbines and other machines can be investigated through noncontact with the rotor. The present experimental results are obtained using the magnetic bearing test rig in the Corporate Applied Research Laboratory of the Ingersoll-Dresser Pump Company. This rig contains three magnetic bearings, two of which sense radial forces and one which senses axial thrust (figures 3 and 4).

The impeller (figure 2) is mounted on the main shaft of the rig (figure 5). The rotor is suspended in a magnetic field generated by magnets mounted around the rotor. A control circuit (figure 6) is used to alter the current in the coils and hence the magnetic field in response to the shaft positions which are sensed by the proximity probes. The bearing force is directly inferred from the magnetic bearing current and rotor position.

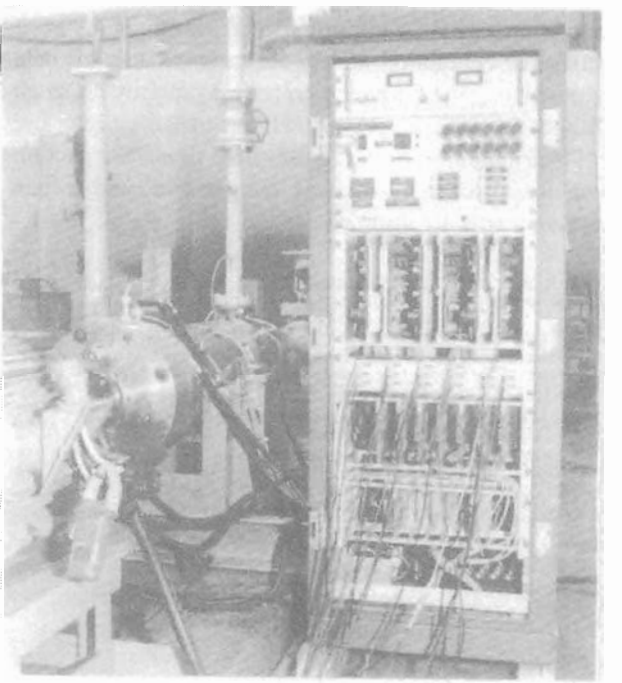

FIGURE 4: Control Unit for the Magnetic Bearing Test Rig at Ingersoll-Dresser Pumps.

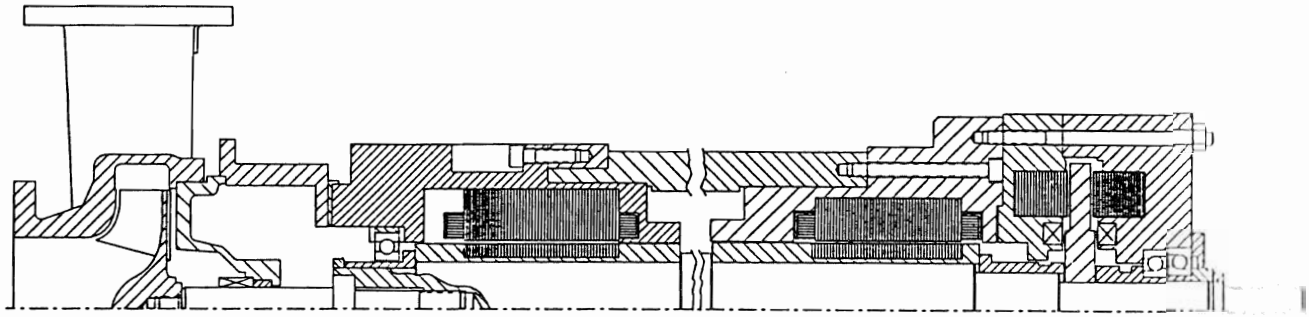

FIGURE 5: Schematic of the Magnetic Bearing Test Rig at Ingersoll-Dresser Pumps. Note the locations of the two Radial and single double-acting axial magnetic bearings.

This allows identification of the radial impeller forces, axial impeller force and impeller moments. Thus, the magnetic bearings serve two functions: to keep the rotor centered in the stator and to act as force sensors.

Each radial bearing has 2 displacement sensors arranged 90 degrees apart. One axial displacement sensor is used for the control of the axial bearing. In addition 4 axial sensors, spaced 90 degrees apart are located on a disk behind the impeller. These latter probes give a qualitative indication of the hydraulic moment and verify the calculation of the impeller moment inferred from the forces at the magnetic bearings. A shaft encoder provides a once per revolution signal. A multiplier increases the number of pulses per revolution and is the trigger pulse for data acquisition. This limits the errors associated with small changes in shaft speed. In addition to the current and displacement signals being sampled, flow rate, suction pressure, discharge pressure, temperature, and torque measurements are sampled.

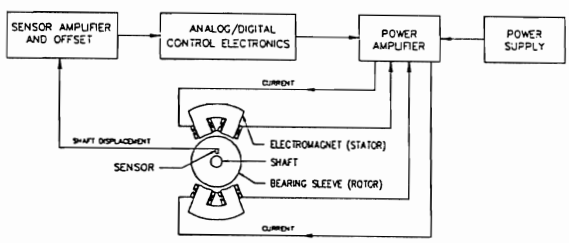

FIGURE 6: Schematic of the Magnetic Bearing Control Scheme.

Impeller Force Calculation

The bearing reaction can be calculated from the measured currents and displacement. The force equation for a single axis of a magnetic bearing is a nonlinear function of the current in the coils and the rotor displacement:

$$F = \mu_0 c_g A_g N^2 \left[\left(\frac{i_A}{c_A} \right)^2 - \left(\frac{i_B}{c_B} \right)^2 \right] \quad (5)$$

where

A_g is the cross- sectional area of the flux path

c_g is a geometry correction factor.

c_A, c_B represent the top and bottom effective radial clearances in the axis.

i_A and i_B represent the current in the top and bottom magnet pair.

N is the number of turns per magnet.

μ_0 is the permeability of free space, ($4\pi \times 10^{-7}$ H/m).

Before the forces at the impeller can be determined, a bearing bias force correction and offset calibration must be made. The procedure involves applying a known force to the bearing axis such as the component of weight supported by that axis. This is done by levitating the shaft at the start of each experiment to determine the actual top and bottom effective clearances, for each bearing axis, c_A and c_B. The magnetic bearing actuators and sensors are not collocated axially, however this position error is accounted for in the analysis procedure. Using this result as well as the measured currents and displacements, the bearing reaction force is calculated as a result of the applied forces and moments on the impeller. The radial impeller forces are determined by summation of forces and moments obtained at the bearings. The impeller thrust force is assumed to be that measured at the thrust bearing. The impeller moments are determined by summation of moments at the impeller centerline.

Calibration

The bearings have a radial force capacity of 6 672 N each and an axial force capacity of 35 584 N in either direction. A loading fixture has been designed and is used to determine the relationships between the bearing currents and impeller forces via static calibration. Thus the reactions of the loads at the bearings are calculated and compared to the known applied loads. The loading procedure included loading the shaft with a couple. A hysteresis curve was also generated and found not to be significant. It has been found that the calibration is independent of operating speeds.

RESULTS

The objective of this test rig (figure3) is to determine the relationship between the geometry, different operating conditions and the hydraulic forces. This magnetic bearing test rig has been designed to evaluate the forces and moments for a wide range of commercial pumps. The initial test utilizing this rig is of a single stage end suction process pump with a semi-open impeller. In this configuration, the maximum radial load at the impeller is 2 224 N. The pump characteristics for a typical 7 bladed centrifugal pump and installed in a well-matched single spiral volute are as follows:

Table 2: The pump characteristics (figure2).

head at 3550 RPM	120 m
flow at 3550 RPM	91m^3/h
speed range	1180-3550 RPM
power rating	7.5 - 45 kW

In the paper we present the comparison between the results for the single stage pump obtained by the traditional methods and those derived from magnetic bearing reactions. The results are given for the full range of flowrates from shutoff to runout. The test operating speed was 1790 RPM.

In figures 7 and 8 typical experimental measurements are presented nondimensionalized by $\rho \pi \omega^2 b_2 R_2^3$

where

ρ is the fluid density.

ω is the rotor speed.

b_2 is the width at the impeller discharge.

R_2 is the radius at the impeller discharge.

The variation of the radial forces is shown to be a strong function of flow. At shutoff, the radial force is a maximum; at BEP a minimum.

Table 3: Predicted and measured nondimensional radial forces.

Method	0% flow	50% flow	100% flow
Stepanoff	0.145	0.113	0
Agostinelli ...	0.05	0.022	0.003
Biheller	0.021	0.016	0
Present data	0.116	0.058	0.014

At shut-off, the Agostinelli et al. (1960) and Biheller (1965) empirical methods under-predict the radial load, whereas the Stepanoff method gives a high value. This has been an observation among pump designers even when the impeller is closed and the geometry is simple, such as no scallops. It is also noted that even at BEP, a radial load is present. The prediction of the axial load by the empirical relation of Stepanoff(1957) yields a nondimensionalized value of 1.12 compared with the presently obtained results of 0.404. This discrepancy is not too surprising as the scalloped region is not accounted for. The method of the Hydraulic Institute, given by equation (4) predicts a value of 0.6

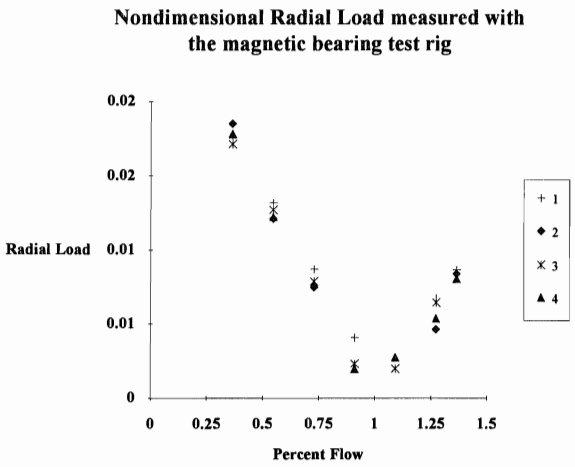

FIGURE 7: Nondimensionalized Radial Forces measured with the Magnetic Test Rig. Series 1 and 3 were measured for decreasing flow; series 2 and 4 were for increasing flow.

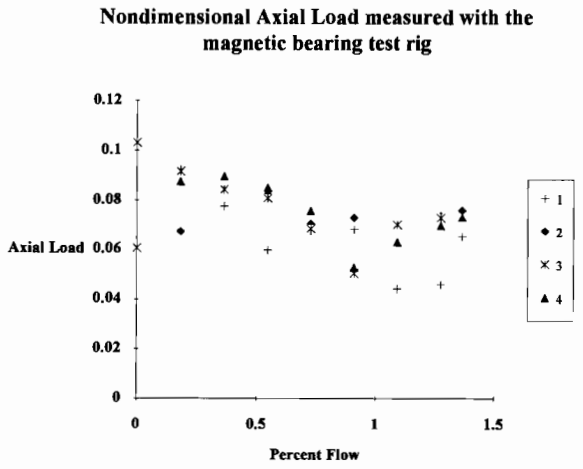

FIGURE 8: Nondimensionalized Axial Forces measured with the Magnetic Test Rig. Series 1 and 3 were measured for decreasing flow; series 2 and 4 were for increasing flow.

CONCLUSIONS

The emphasis of this paper is to investigate the steady forces acting on the rotor and casing due to fluid flow in a centrifugal pump with a new load measuring concept. In the paper we have presented the comparison between the results for a single stage pump obtained by the traditional methods and those derived from magnetic bearing reactions. Empirical relationships which do not account for the impeller geometry do not accurately predict the impeller forces. A knowledge of the fluid forces can thus avoid radial/axial bearing failures. In the future, the same magnetic bearings will be used to evaluate steady and fluctuating loads in larger, multistage pumps.

ACKNOWLEDGMENTS

The authors would like to thank the management of Ingersoll-Dresser Pump Company for granting permission for publication, and in particular Mr Ian Massey and Dr. Paul Cooper. We would also like to thank Dr. Joe Imlach of Imlach Consulting Engineering and those from Kingsbury, Inc. who participated in this project.

REFERENCES

1. Adkins, D. R., Brennen, C. E. 1988. Analyses of Hydrodynamic Radial Forces on Centrifugal Pump Impellers, ASME J. of Fluids Eng., Vol.110, pp. 20-28.
2. Agostinelli, A., Nobles, D. and Mockrige, C.R. 1960. An experimental Determination of Radial Thrust in Centrifugal Pumps, J. of Eng for Power., Vol.82, pp. 120-126.
3. Biheller, H.J. 1965., Radial Force on the Impeller of Centrifugal Pumps with Volute, Semivolute, and Fully Concentric Casings, ASME J. of Eng. for Power., July 1965, pp. 319-323.
4. Bolleter, U., Wyss, A., Welte, I. and Sturchler, R. 1985. Measurements of Hydrodynamic Interaction Matrices of Boiler Feed Pump Impellers, ASME Paper No. 85-DET-148.
5. Buse, F.W. The Hydraulic Couple. Ingersoll-Rand Company internal publication. July 1979.
6. Domm, U. and Hergt, P. 1970. Radial Forces on Impeller of Volute Casing Pumps. Flow research on Blading, Editor L.S. Dzung, Elsevier Publ. Co., Netherlands, pp. 305-321.
7. Chamieh, D.S., Acosta, A.J., Brennen, C.E. and Caughey, T.K. 1985. Experimental Measurements of Hydrodynamic Radial Forces and Stiffness Matrices for a Centrifugal Pump Impeller. ASME J. of Fluids Eng., Vol. 107, No. 3, pp. 307-315.
8. Hergt, P. and Krieger, P. 1969-70. Radial Forces in Centrifugal Pumps with Guide Vanes. Proc. Inst. Mech Eng.., Vol. 184, Part 3N, pp. 101-107.
9. Iversen, H.W., Rolling, R.E. and Carlson. Volute Pressure Distribution, Radial Force on the Impeller, and Volute Mixing Losses of a Radial Flow Centrifugal Pump. J. of Eng. for Power. vol 82, pp. 136-144.
10. Jery, B., Acosta, A.J., Brennen, C.E. and Caughey, T.K. 1985. Forces on Centrifugal Pump Impellers Second International Pump Symposium, Houston, TX, April 29 - May 2 1985.
11. Ohashi, H., Sakurai, A., Nishihama, J. Influence of Impeller and Diffuser Geometries on Lateral Fluid Forces of Whirling Centrifugal Impeller. 4th Workshop on Rotordynamic Instability Problems in High-Performance Turbomachinery. Texas A&M University, College Station, TX, 16-18 May 1988.
12. Ohashi, H., Shoji, H., 1987, Lateral Fluid Forces on a Whirling Centrifugal Impeller (2nd Report; Experiment in Vaneless Diffuser), ASME J. of Fluids Eng, Vol. 109, No2., pp.100-106.
13. Stepanoff, A.J. 1957., Centrifugal and Axial Flow Pumps, John Wiley & Sons, Inc. New York, N.Y., pp. 116-123.